Materials Science and Engineering B 300 (2024) 117016

Contents lists available at ScienceDirect

Materials Science & Engineering B

journal homepage: www.elsevier.com/locate/mseb

Physicochemical factors that enhance the third order nonlinear susceptibility $\chi^{(3)}$ in nitroanilines and conjugated polyenyne polymers with arylamine substituents

C.A. Guarin [a,c], L.G. Mendoza-Luna [a,c], J.L. Hernández-Pozos [a], J.A. Díaz-Ponce [a,b,*]

[a] Departamento de Física, Universidad Autónoma Metropolitana-Iztapalapa, Av. San Rafael Atlixco 186, Col. Vicentina, Apdo, Post. 55-534, Mexico City C.P. 09340, Mexico

[b] Postdoctoral Position, Universidad Autónoma Metropolitana-Iztapalapa, Av. San Rafael Atlixco 186, Col. Vicentina, Apdo, Post. 55-534, Mexico City C.P. 09340, Mexico

[c] Cátedras CONACYT – Departamento de Física, Universidad Autónoma Metropolitana Iztapalapa, Av. San Rafael Atlixco No. 186 Col. Vicentina, C.P. 09340 México D. F., México

ARTICLE INFO

Keywords:
Nitroanilines
Aromatic polyenynes
Correlation effects
NLO properties
Hückel's model

ABSTRACT

This work analyzes the physicochemical factors that improve the $\chi^{(3)}$-NLO properties based on Hückel-Agrawal's model. The model compounds are the nitroanilines ortho o-NA, meta m-NA, and para p-NA, and the aromatic polyenynes with phenyl and an NH_2 group in position ortho, meta, and para, or without the amine group. We analyze the correlation effects, the dipole moments, the resonance energy, the frequency of the laser wavelength, the interband and intraband effects, the charge density, the curvature of the dipole moments, and the vibration phononic factor in addition to the molecular effects proposed by Nalwa's work. Then, we have found, for example, that the addition of a conjugate chain to the nitrogen of the amine, the continuity of the same sign of charge in the valence band, which produces electric repulsion, or the increase in the spatial asymmetry of the groups attached to the aromatic ring can increase the $\chi^{(3)}$ values.

1. Introduction

The nonlinear optical (NLO) properties of the materials can improve the communication and storage qualities of the electrooptic devices. Several factors that can improve these properties are a low band gap edge [1a], a low dimensionality [2], a high transition dipole moment [2], and high electronic delocalization in conjugated polymers [1a,2]. Based on Hückel-Agrawal's methodology, we can include a low resonance energy β_2, a high difference in the Brillouin zone between the ground and excited dipole moments Ωvv and Ωcc, respectively [1a], and the high variation of the transition dipole moments Ωcv and Ωvc in the Brillouin zone (intraband contribution) [1a], high value of the molecular surface density σ, [1a], resonance in the one photon, i.*e.*, $+\omega-\omega+\omega$ *or* $+\omega+\omega-\omega$, and three-photon $-\omega-\omega-\omega$, mainly, frequencies [1a,3,4].

One of the problems in the increment of the $\chi^{(3)}$-NLO properties is the oscillations of $\chi^{(3)}$ values in the Brillouin zone, which nullifies high values of $\chi^{(3)}$ [3]. Increasing the molecular asymmetry of the molecular wavefunctions avoids these oscillations. Indeed, the highest curvature (2nd derivative) of the wavefunction coefficients increases the NLO properties as analyzed by the equations of dipole moment deduced by Guarin and Díaz-Ponce [3,4]. In this fashion, the aromatic polyenynes with aniline in the para position have a second derivative of the wavefunction coefficients of the order of 10^7 [5].

In this work, we perform a quantitative analysis of the physicochemical effects that enhance the nonlinear optical (NLO) properties of nitroanilines and related aromatic polyenynes. Additionally, we provide a methodology for evaluating the correlation effects within the nitroanilines. Also, we analyze the 3-dimensional 3*D* effects of the charge and dipole moments in the NLO properties. Indeed, the dipole moment $\mu = Q(a_1x, b_1y, c_1z)$ weighs the 3*D* directions ×, y, and z over the charge Q. This analysis is beside the evaluation of the one-dimensional 1*D* Agrawaĺs equation. We also predict high $\chi^{(3)}$ values from the high values of the second derivative of the wavefunction coefficients' real and imaginary number parts. Also, we analyze the defocusing behavior in

* Corresponding author at: Departamento de Física, Universidad Autónoma Metropolitana-Iztapalapa, Av. San Rafael Atlixco 186, Col. Vicentina, Apdo, Post. 55-534, Mexico City C.P. 09340, Mexico.

E-mail address: qjavier2002@yahoo.com (J.A. Díaz-Ponce).

https://doi.org/10.1016/j.mseb.2023.117016
Received 11 September 2023; Received in revised form 9 November 2023; Accepted 11 November 2023

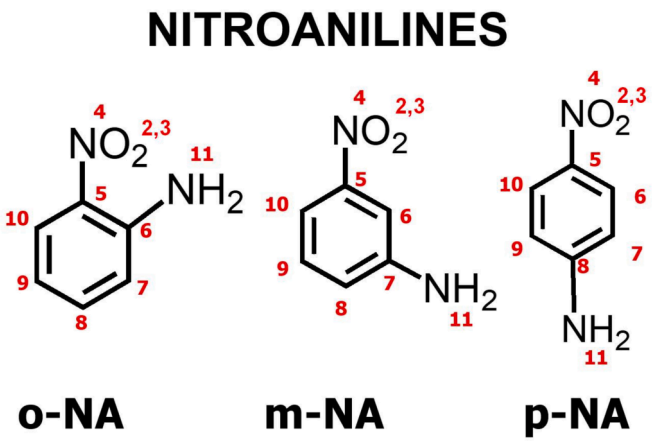

Scheme 1. Structures of the nitroanilines.

Table 1
Model compounds for the aromatic polyenynes.

Acronym	Nomenclature	Scheme
POEBz	Poly[but-2-yn-1,4-diylene)benzene]	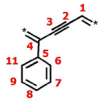
POEo-A	Poly[2-(but-2-yn-1,4-diylene)aniline]	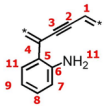
POEm-A	Poly[3-(but-2-yn-1,4-diylene)aniline]	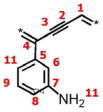
POEp-A	Poly[4-(but-2-yn-1,4-diylene)aniline]	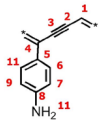

nitroanilines because this characteristic in the materials avoids heating of waveguides.

2. Methodology.

2.1. Compounds

Scheme 1 shows the structures and notations of the model compounds nitroanilines:

The NH_2 aromatic polyenynes are other model compounds built of a polyenyne moiety and an NH_2-substituted phenyl moiety. Table 1 shows these aromatic polyenynes:

We used Agrawal's methodology for the energy and wavefunction evaluation of the nitroanilines and aromatic polyenynes. We found double degeneracy for the nitroanilines and single degeneracy in the conduction bands for the aromatic polyenynes, as seen in **Figs. S1 and S2**. We used the Fermi Golden factors based on Agrawal's model, as explained in References [4,5], for all the compounds evaluated in this work. In the case of the nitroanilines, there was a high proximity of the calculated $\chi^{(3)}$ values to the experimental ones. This closeness of the values is worthwhile because the equations of the $\chi^{(3)}$ values have an

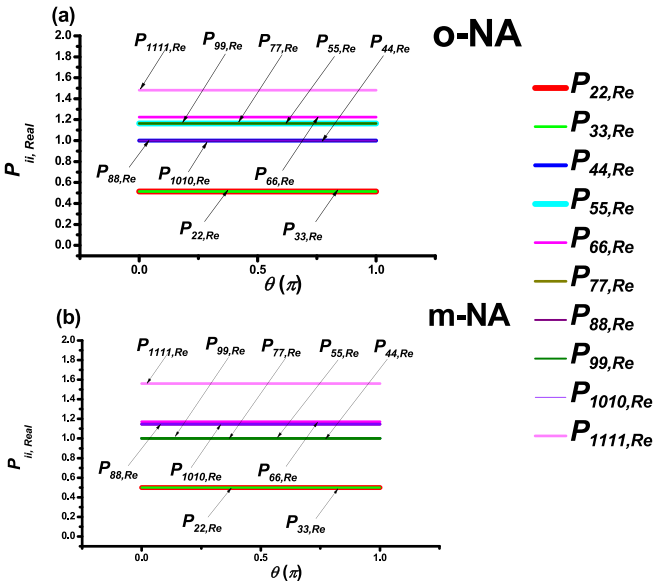

Fig. 1. The mobile bond order factors on atom i, *Pii*, for a). o-NA, b). m-NA.

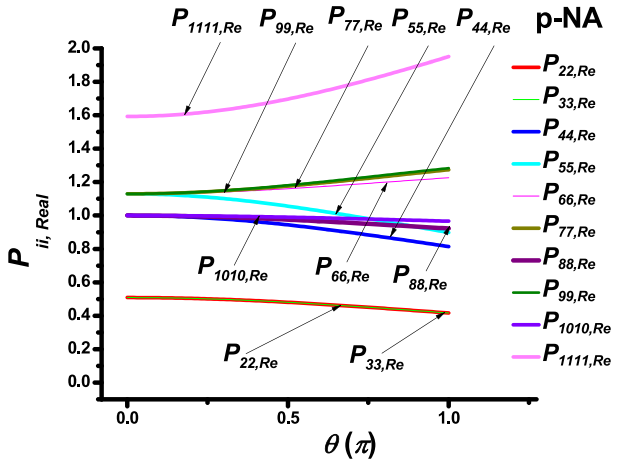

Fig. 2. The mobile bond order factors on atom i Pii for p-NA.

intricate formulation because of the Fermi Gold Rule, as seen in **Eqs. (14), (15), (18), and (19)** in **Appendix A**.

2.2. Correlation Effects

We have evaluated the correlation effects only for the nitroanilines through Pople's model [6], which considers the effect of the *Pij* factors in the standard Hückel's model. We do not evaluate the correlation effects in the aromatic polyenynes. We have found that in o-NA and m-NA, the correlation *Pii* factors are constant throughout the Brillouin zone, with *Pii* imaginary equal to 0 and *Pij* equal to 0. This constancy of the values simplifies the evaluation of the linear and NLO optical properties. These *Pii* factors are plotted in Fig. 1 for both nitroanilines, considering that no correlation effects imply $Pii = 1$. This no-correlation effect happens in N4, C8, and C10 for the o-NA, as shown in Fig. 1a, and in N4, C5, C7, and C9 for m-NA, as shown in Fig. 1b. Also, atoms N11, O2, and O3 in o-NA and p-NA present more remarkable correlation effects, as observed in Fig. 1a and 2. In nitrogen, the correlation effect is up, and in the oxygens, it is down, as seen in these figures. As observed, the carbons attached to the nitrogens of the nitro and amine in o-NA have up-correlation effects: C5 and C6, respectively. Conversely, the respective carbons (C5 and C7) in m-NA do not have correlation effects. This analysis changes when we

consider the experimental bond lengths of o-NA and m-NA, which indicate these anilines' most critical resonance states with the corresponding correlation states associated with each carbon, as explained below.

On the other side, the mobile bond order factors on atom i, *Pii*, of the p-NA varies in the Brillouin zone, which produces a nonconstant J-K/2 value throughout the Brillouin zone, at the difference of the o-NA and m-NA. The values of *Pij* for p-NA are given in Fig. 2. In the case of p-NA, the J-K/2 values are for $\theta = \pi$. As observed in Fig. 2, the correlation effects decrease at large distances (θ=0), with a value of no correlation effect in C4, C8, and C10. The higher-up correlation effect is with the nitrogen atom N11, and the higher-down correlation effect is in the oxygens O2 and O3. Remarkably, the symmetric carbons of the aromatic ring (C6 and C10) do not have similar correlation effects; this is not the case for C7 and C9, whose correlation effects are similar. The reason that the values of C5 and C10 are not similar is that the absolute values of the energies E1 = 0, E2 = 0, E6, E7 are equal, that is, |C6| = |C10|, but in the other energies |C6| ≠ |C10| and then that is the reason of different behavior.

In order to evaluate these factors, we used Kopineck's tables [7], in which we also included the evaluation of the interaction of onsite and near-site bond correlations J-K/2. In the Supplementary Information, Schs. S1, S2, and S3 show the primary resonant structures for evaluating the correlation effects. For example, the bond lengths in the crystalline structure of p-NA [8] indicate that the aromatic ring has fixed single and double bonds, which indicates a hydro compound that has two possibilities shown in Sch. S3, one is an anion in carbon C5 (Sc. S3a), and the other is a double bond between the carbon C5 and the nitrogen N4 (Sc. S3b). As Pariser and Parr [9] considered, J-K/2 values must have several figures of precision because the evaluation of the wavefunction coefficients Ci varies noticeably with a variation of the resonance energy β_2 and the values of J-K/2. For this reason, we have digitalized Kopineck's tables. In this way, **Table S1** of the Supplementary Information tabulates the values of J-K/2. When we assume that there is an anion in C5 (Sch. S3a in the Supplementary Information), the correlation effects of O2 and O3 are similar to the correlation effects of C5 and N4 in the case of a possible double bond between C5 and N4 (Sch. S3b in the Supplementary Information). **Figs. S3 and S4** show this behavior, respectively, in the Supplementary Information. Also, when we assume an anion in C5 (Sch. S3a), the effect of N4 is considerable and zero for C5 (**Fig. S3** in the Supplementary Information). In the case of a double bond between C5 and N4 (Sch. S3b), there is a low value of O2 and O3 (**Fig. S4** in the Supplementary Information). This low value, in principle, is not physicochemical correct by the resonance between nitrogen and the oxygens: One expects a switching of the double and single bond to the nitrogen between the oxygens. Then, case b is not possible to happen. However, evaluating the $\chi^{(3)}$-NLO properties considering the double bond of the nitrogen N4 with the carbon C5 gives a $\chi^{(3)}$ value of 86 % of the experimental one.

Conversely, the case of the presence of an anion in C5 gives values ≫ 150% more than the experimental one. Then, the case of a primary resonance with a double bond between carbon C5 and nitrogen N4, with single bonds between this nitrogen and the oxygens, is more plausible by the $\chi^{(3)}$-NLO properties. Besides, we have evaluated the secular equations by adding the variation in the correlation effect for the particular energy value only for the specific wavefunction coefficient. Adding the correlation effect only to the energy value reduces the time to find better values of the wave function coefficients in the calculations. The calculated values of the wavefunction coefficients produce values of $\chi^{(3)}$ that are close to the experimental values. Appendix SA of Supporting Information shows an example of the secular equations, in this case, for the valence band of m-NA. We must also explain that there is no correlation effects in the energy $E = 0$.

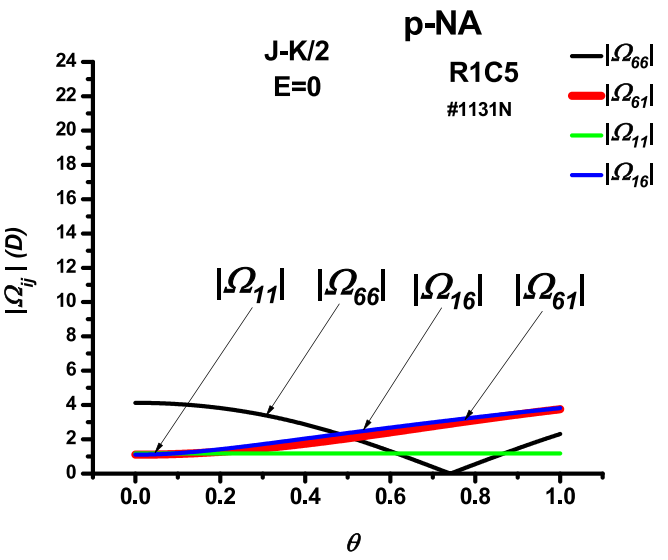

Fig. 3. Variation of the dipole moment in p-NA along the pseudo-Brillouin zone due to correlation effects.

2.3. Dipole Moments

We have estimated the ground state μ_g and excited state μ_e dipole moments through the quantum vector method. This method evaluates the dipole moments of the σ-bonds and the π-bonds to calculate the total dipole moment [10]. The σ dipole moment contribution comes from the hybridization and bond moments due to the difference of electronegativity with inductive effects associated with bond overlaps, in which lone pairs and core polarization have a high weight in the dipole moment value. The π bonds have the same background. Then, we have two contributions to the dipole moment: a σ contribution (σ bond) and a π contribution (π bond). In this way, we used the charge density Ci^2 of the π orbitals to evaluate a similar contribution to the σ dipole moment. Besides, the charge of the oxygens O2, O3, and nitrogens N4 and N11 were changed in the σ contribution in order to adjust the calculated dipole moments to the experimental ones.

3. Results and discussion

Table S2 of Supplementary Information shows that the value of the resonance energy β_2 is almost equal for the correlated case compared to the uncorrelated cases. This similarity of the resonance energies β_2 implies that the gaps are similar, as seen in **Eq. (1)**; then, the absorption maxima do not change appreciably by the correlation effects:

$$E = h\omega_{cv} = 2\pi\beta_2\,(\zeta_c - \zeta_v) \tag{1}$$

where ω_{cv} is the frequency of the band gap.

The effect of the correlation effects in the dipole moments, on the contrary, is so different from the uncorrelated case. In this way, the intraband contribution changes appreciably due to the variation of the dipole moments, as seen in Fig. 3 for p-NA in R1C5 compared with **Fig. S8** of Supporting Information. Indeed, the absorption maxima in p-NA depend only on the transition dipole moment Ωcv, c = 1, v = 6, not on the other dipole moments, as observed in **Eqs. (20) and (21)**, but the influence of the correlation effects on the absorption maximum is zero, as observed in the resonance energies of **Table S2** for p-NA, as explained above.

On the other hand, the evaluation of the values of $\chi^{(3)}$ for the nitroanilines in **Reference** [4] considered a value of the surface molecular density σ of 1.99 X 10^{13}, similar to the β-carotene, which was obtained in **Reference** [3]. Now, we have evaluated the value of σ of the crystal of the nitroanilines, and it gives high values of σ. The evaluation

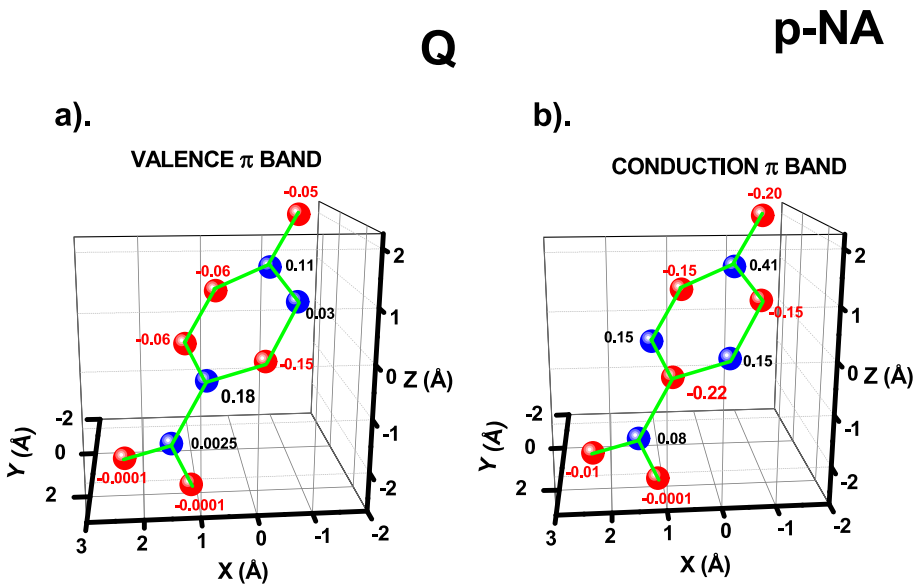

Fig. 4. The charge distribution in p-NA considering correlation effects in the a). valence, and b). conduction band. As observed in the valence band, there are nearer atoms with the same charge sign. This nearer charge of the same sign produces instability in the valence band because of the electric repulsion. In the conduction band, all the nearer atoms change sign. This change of sign produces stability, and then the dipole moment increases.

Table 2
Number of nearer atoms with the same sign of charge.

	Valence Band		Conduction Band	
	# Nearer atoms	ΔQ	# Nearer atoms	ΔQ
Nitroanilines				
o-NA	4	0.44	0	–
m-NA	0	–	3	0.00
p-NA	6	0.45	0	–
Aromatic Polyenynes				
POEBz	3	0.05	3	0.05
POEo-A	6	0.30	0	–
POEm-A	6	0.41	6	0.42
POEp-A	6	0.41	0	–

Table 3
Change of sign of the charge between the valence and conduction band.

	Changes of signs
Nitroanilines	
o-NA	3
m-NA	7
p-NA	4
Aromatic Polyenynes	
POEBz	0
POEo-A	8
POEm-A	3
POEp-A	8

considers that the length of the unit cell is 3a, which encompasses the aromatic ring and then the molecule. Table S2 of **Reference** [5] report these values.

3.1. Atomic charge

There is a correlation in the increase of the NLO properties related to the charge in the nitroanilines and aromatic polyenynes in three concepts:

(1) The conduction band has less continuity in the same sign of charge for nearer atoms in the molecule than the valence band: A more stable configuration has a change of sign of the charge in nearer atoms and a similar charge. On the opposite, the continuity of the same sign in the nearer atoms makes the structure unstable by the electric repulsion. This continuity of the sign of the charge in the valence band is accomplished, for example, in the nitroaniline p-NA in which six nearer atoms have the same sign of charge *Q* in the valence band, and 0 nearer carbons have the same sign of charge in the conduction band as seen in Fig. 4. Then the tendency is to a higher transition from the valence band to the conduction band. Table 2 shows the number of nearer carbons with the same charge #Nearer atoms in valence and conduction bands. Also, Table 2 reports the absolute value of the charge of the nearer atoms ΔQ.

Table 4
Change of charge from the valence to the conduction band in the carbon C5 **ΔQcv(C5)** joined to the nitro (NO_2) or enyne group.

	Q		ΔQcv (C5)	ΔQcv (NO_2)	ΔQcv (aromatic ring + N11)
	Valence Band	Conduction Band			
Nitroanilines					
o-NA	−0.09	−0.24	−0.15	0.01	0.15
m-NA	−0.09	0.15	0.24	0.01	−0.22
p-NA	0.18	−0.22	−0.40	0.07	0.33
Aromatic Polyenynes				ΔQcv (Enyne)	
POEBz	−0.02	−0.02	0.00	0.00	0.00
POEo-A	0.06	−0.23	−0.29	0.11	0.17
POEm-A	0.11	0.15	0.04	0.01	−0.05
POEp-A	0.11	−0.18	−0.29	0.13	0.16

(2) We consider that the higher continuity of sign of charge in p-NA in the valence band, for example, makes the transition to the conduction band more likely, as seen in Fig. 4.

(3) A preferred tendency to change the sign of the charge from the valence to the conduction band: This is obvious because the sign change attracts the charge from the valence band to the conduction band. Table 3 shows the signs change in nitroanilines and

Table 5
Charge density Ci^2 of the nitrogen N11 in the valence and conduction band.

	Ci^2 in N11		ΔCi^2 (N11)
	Valence Band	Conduction Band	
Nitroanilines			
o-NA	0.10	0.48	0.38
m-NA	0.06	0.56	0.50
p-NA	0.20	0.54	0.34
Aromatic Polyenynes			
POEBz	–	–	–
POEo-A	0.00	0.43	0.43
POEm-A	0.10	0.56	0.46
POEp-A	0.08	0.56	0.48

aromatic polyenynes, not considering the charge 0.00 as the change of sign. Fig. 4 shows this behavior for p-NA.

(4) If we consider the transition from the valence band to the conduction band, when the change of charge in the carbon C5 in this transition is towards a negative charge, the more is the change towards a positive charge in the aromatic ring plus the nitrogen N11 (loss of negative charge or increase of positive charge) and the opposite. The change to the negative charge of carbon C5 correlates with high NLO values or the opposite. In this case, the carbon C5 operates as negative or positive charge reservoir. Also, in the case of nitroanilines, the group nitro in p-NA gives up more of its charge to carbon C5 but not in o-NA and m-NA, as seen in Table 4. This table also shows that the effectiveness of the group nitro of POEo-A and POEp-A to give up its charge is similar.

Furthermore, Table 4 shows that the aromatic ring plus the nitrogen N11 group in nitroanilines gives up more electronic charge in this transition and not so much in the nitro group. On the other hand, similarly, in the aromatic polyenynes POEo-A and POEp-A, both the aromatic ring plus the nitrogen N11 and the enyne group give up their charge to the carbon C5. Concerning the nitroaniline m-NA and the aromatic polyenyne POEm-A, the carbon C5 and the nitro group decrease their electronic charge in order to transfer it to the aromatic ring plus the N11 nitrogen. This transfer of charge to the aromatic ring plus the N11 is the reason for their low NLO property values.

3.2. Charge Density Ci^2

About the charge density associated with the square of the wavefunction coefficient Ci^2, we have found three characteristics associated with the transition from the valence to the conduction band:

(1) There is an increase of the charge density Ci^2 in the transition from the valence band to the conduction band in the nitrogen of the amine N11, as seen in Table 5, with the concomitant high increase of charge density Ci^2 in the conduction band. In this way, the charge density Ci^2 in N11 in the conduction band is from 0.43 in POEo-A to 0.56 in m-NA, POEm-A, and POEp-A. This charge density increase from the valence band to the conduction band in N11 opens the possibility of adding a conjugated chain to the nitrogen N11 in order to disperse the charge and increase the conjugation.

(2) The atom joined to the nitrogen of the amine in the conduction band has a charge density of $Ci^2 = 0$ for all the compounds, as observed, for example, in Fig. 5b for p-NA.

(3) The charge density Ci^2 of the conduction band in the nitro group of the nitroanilines and the enyne group of the aromatic polyenynes is low: $Ci^2 \leq 0.04$ and $Ci^2 \leq 0.13$, respectively, except for POEBz, as seen in Table 6. This charge density Ci^2 decrease is a function of the aromatic ring: decrease of the charge density Ci^2 in the nitro or enyne groups in order to increase the conjugation. Another exception in the decrement of charge from the valence to

Table 6
Charge density Ci^2 of the nitro or enyne group in the valence and conduction band.

	Ci^2 in N11		ΔCi^2
	Valence Band	Conduction Band	
Nitroanilines	**Nitro group**		
o-NA	0.07	0.04	−0.03
m-NA	0.47	0.00	−0.47
p-NA	0.00	0.02	0.02
Aromatic Polyenynes	**Enyne group**		
POEBz	0.53	0.53	0.00
POEo-A	0.52	0.13	−0.45
POEm-A	0.33	0.00	−0.33
POEp-A	0.60	0.07	0.53

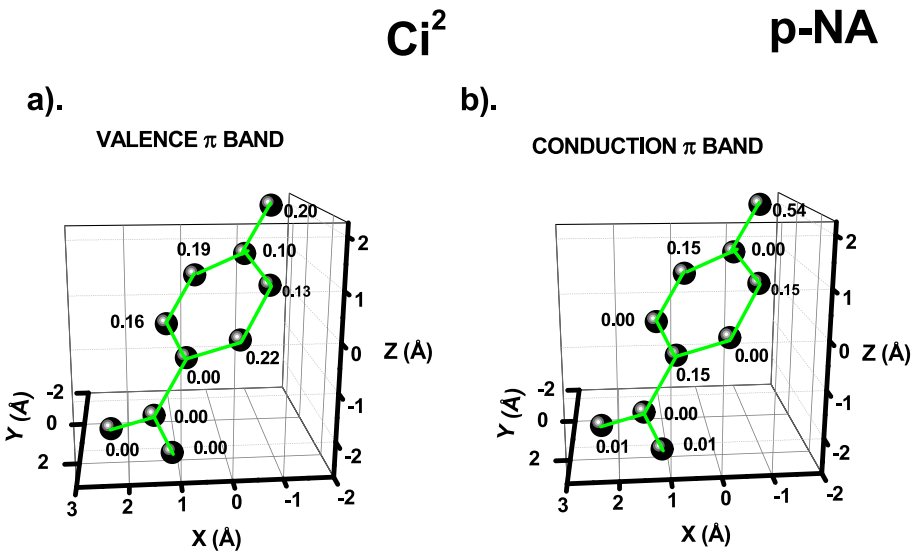

Fig. 5. Charge density Ci^2 of the a). valence, and b. conduction bands of p-NA. In the valence band, zero-density charge density in the nitro group, the presence of charge density in the carbon joined to the nitrogen N11 of the amine and low charge density in the nitrogen N11. On the other side, in the conduction band, low charge density in the nitro group, zero-charge density in the carbon C8 joined to the nitrogen N11 and high concentration of charge density Ci^2 in the nitrogen N11.

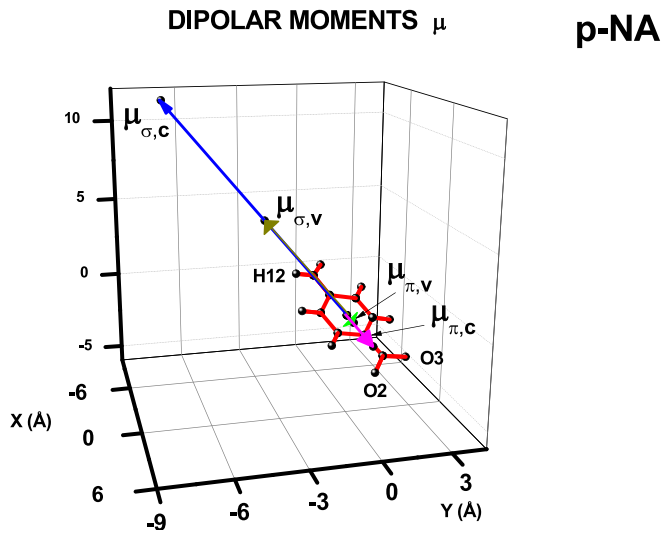

Fig. 6. Dipole moments μ_σ and μ_π for the valence and conduction bands for p-NA.

the conduction band is in the nitro group of p-NA. However, this nitro group of p-NA already has a low charge density Ci^2 in the valence and conduction bands, as observed in Fig. 5a,b.

3.3. Dipole Moment

We found that the σ and π contributions to the dipole of the p-NA are in the same direction through the symmetry axis of this molecule passing through the two nitrogens, as seen in Fig. 6. This direction produces perturbations of the electronic cloud, mainly because the nitrogen N11 has a change of charge in the transition from the valence to the conduction band, as explained above, allowing applying poling [11] in this material the increase of the NLO properties. In the o-NA and m-NA, the dipole σ and π dipole moments are in different directions, as seen in **Figs. S5 and S6**, poling is less practical than in p-NA. In **Table S3** of Supplementary Information are reported the absolute values of the σ and π dipole moments in the valence and conduction band and the charges associated with the nitrogen N11 of the amine to adjust the values of the σ dipole moments to be near the total dipole moment of the experimental ones.

3.3.1. Equation of Dipole Moment

Appendix A exposes the wavefunction equations and the associated dipole moments. In this way, we can associate the interband part of the dipole moment Ωvv to the charge density associated with the square of the wavefunction coefficient Civ^2. In o-NA, as a simple molecule, the correlation effects do not produce almost a change of the dipole moment in the pseudo-Brillouin zone, as observed in **Fig. S7**. Then, the charge density of the wavefunction coefficients Ci^2 gives the total dipole moment in each case of the ground and excited states, see as comparison **Eq. (11)**. Also, in this case, the normalized average transition dipole moment $\Omega_{i,cv}/(a_{ver}\ e)$ in the atom i, by its part, is associated to

$$\Omega_{i,cv}/(a_{aver}e) = (c^2_{ic,aver} * c^2_{iv,aver})^{0.5} \quad (2)$$

then, we can calculate the weight of each atom in the transition dipole moments in the interband contribution, as seen in Table 7. We must clarify that the dipole moments consider the influence of several atoms, as seen in **Eqs. (11)** and **(13)**, weighted by numerical factors, and that, in this case, we only analyze the interband contribution, as specified above. In the case of the intraband contribution, the high NLO values for p-NA and all the aromatic polyenynes are due to the high change of the dipole moment along the Brillouin zone in p-NA and the aromatic polyenynes, as seen in Figs. 3 and S9 of Supplementary Information, respectively. In m-NA, the dipole moment changes not appreciably in the Brillouin zone, as seen in **Fig. S10** of Supplementary Information, then both interband and intraband contributions have weight.

As observed in Table 7, nitrogen N11 has the principal influence on the transition dipole moments $\Omega_{i,cv}/(a_{ver}\ e)$ of all compounds. In the nitroanilines o-NA and p-NA, the atoms near the carbon joined to the nitrogen N11 of the group amine have more weightiness on the transition dipole moments $\Omega_{i,cv}/(a_{ver}\ e)$. In m-NA, the atoms C6, C8, and C10 have significance on the transition dipole moments $\Omega_{i,cv}/(a_{ver}\ e)$ because they are different from zero, having the most influence on the latter two. Indeed, by **Eq. (2)**, we realize that if the wave density Ci^2 of the valence band or the conduction band is zero, the transition moment is zero. Then, o-NA has more atoms contributing to the transition dipole moment (6). Only 4 atoms contribute to m-NA and p-NA with a zero influence of the nitro group, and, precisely, the nitrogen N4 does not contribute to any nitroaniline. Table 7 gives a proportion of the influence of the atoms in the dipole moment. Also, the symmetry of the valence and conduction band in the pure polyenyne aromatic POEBz does not allow a high transition dipole moment.

For this reason, deleting for the analysis the polyenyne POEBz, the spatial asymmetry of the enyne group, which includes the carbons C1 to C4, has a contribution of $\Omega_{i,cv}/(a_{ver}\ e)$ of 0.20 of the whole 0.42 in POEo-A, 0.00 of the totality 0.56 in POEm-A, and 0.16 of the whole 0.54 in POEp-A, which correlates in the order of the NLO properties as seen in **Table S4** of Supplementary Information. In particular, opposite to the nitroanilines, the nitrogen N11 in POEo-A has a zero value $\Omega_{i,cv}/(a_{ver}\ e)$. POEo-A has as o-NA, p-NA, and POEp-A a value of $\Omega_{i,cv}/(a_{ver}\ e)$ equal to

Table 7
The normalized average transition dipole moment $\Omega_{i,cv}/(a_{ver}\ e)$ in the atom i for the model compounds studied in this work is associated with the interband contribution.

Atom	$\Omega_{i,cv}/(a_{ver}\ e)$ Nitroanilines			Atom	Aromatic Polyenynes			
	o-NA	m-NA	p-NA		POEBz	POEo-A	POEm-A	POEp-A
C1	–	–	–	C1	0.25	0.15	0.00	0.13
O2	0.02	0.00	0.00	C2	0.05	0.00	0.00	0.00
O2	0.02	0.00	0.00	C3	0.10	0.05	0.00	0.03
N4	0.00	0.00	0.00	C4	0.13	0.00	0.00	0.00
C5	0.16	0.00	0.03	C5	0.11	0.10	0.00	0.08
C6	0.00	0.01	0.00	C6	0.08	0.00	0.21	0.00
C7	0.18	0.00	0.14	C7	0.02	0.08	0.00	0.04
C8	0.00	0.08	0.00	C8	0.15	0.00	0.06	0.00
C9	0.02	0.00	0.17	C9	0.03	0.04	0.00	0.05
C10	0.00	0.07	0.00	C10	0.08	0.00	0.05	0.00
N11	0.22	0.18	0.32	N11	–	0.00	0.24	0.21
SUM	0.62	0.34	0.66	SUM	1.00	0.42	0.56	0.54

Table 8
Change of average transition moments in each atom $\Delta\Omega_{i,cv}/(a_{ver}\ e)$ in the atom i for the model compounds studied in this work.

Atom	$\Delta\Omega_{i,cv}/(a_{ver}\ e)$ Nitroanilines			Atom	Aromatic Polyenynes			
	o-NA	m-NA	p-NA		POEBz	POEo-A	POEm-A	POEp-A
C1	–	–	–	C1	0.16	0.15	0.00	0.13
O2	0.02	0.00	0.00	C2	−0.12	−0.10	0.00	−0.08
O2	0.02	0.00	0.00	C3	0.00	0.05	0.00	0.03
N4	−0.07	0.00	−0.01	C4	0.03	−0.08	0.00	−0.06
C5	0.24	−0.03	0.03	C5	0.01	0.10	−0.09	0.08
C6	−0.18	0.01	−0.08	C6	0.02	−0.06	0.21	−0.06
C7	0.18	−0.09	0.14	C7	−0.10	0.08	−0.17	0.04
C8	−0.10	0.08	−0.21	C8	0.13	−0.06	0.06	−0.10
C9	0.02	−0.07	0.17	C9	−0.10	0.04	−0.06	0.05
C10	−0.09	0.07	−0.10	C10	0.02	−0.07	0.05	−0.06
N11	0.22	0.18	0.32	N11	–	0.00	0.24	0.21
SUM	0.25	0.15	0.26	SUM	0.05	0.05	0.25	0.18

zero in the carbon joined to the nitrogen of the amine, which implies that this carbon in these compounds has similar optical behavior. In this analysis, we note that the intraband contribution, given by the variation in 1st and 2nd derivatives of the dipole moment [5], has more than 99 % of the contribution of the $\chi^{(3)}$ values as seen in **Table S4**.

Guarin et al. have [12] considered that a high charge transfer can increase the dipole moments. Besides, we can make the difference in the transition moment of atom i to the ones of the nearer atoms. With this difference, we can evaluate the change of average transition moments in atom i, $\Delta\Omega_{i,cv}/(a_{ver}\ e)$, surrounded by other atoms by the equation:

$$\Delta\Omega_{i,cv}/(a_{aver}e) = \sum_{i+1}^{nearest}\left[\left(c^2_{ic,aver} * c^2_{iv,aver}\right)^{0.5} - \left(c^2_{(i+1)c,aver} * c^2_{(i+1)v,aver}\right)^{0.5}\right] \quad (3)$$

Table 8 reports these values for the nitroanilines and the aromatic polyenynes.

We can associate the value of the change of average transition moments in each atom $\Delta\Omega_{i,cv}/(a_{ver}\ e)$ to the first derivative of the

Table 9
NLO values for o-NA considering the oxygens and nitrogens separated, and also correlation effects.

								Average	% Exp
RIGHT ROTATORY									
Carbon taken as Reference[e]		5	6	7	8	9	10		
λ = 1064 nmb	10^{-13} esu								
	Re $[\chi^{(3)}]$	−11.24	−101.43	−0.00	3.32	−2.05	0.30	−18.52	
	$\lvert\chi^{(3)}\rvert$	11.34	101.57	0.00	3.33	2.05	0.32	18.53	284
	Re $[\chi^{(3)}]$ (-ω-ω-ω)^{1}B	3.16	2.83	0.00	0.93	0.57	−0.09	5.17	
	Re $[\chi^{(3)}]$ (-ω-ω-ω)La	−127.89	−1148.71	−0.24	37.57	−23.22	3.46	−2.10	
	Re $[\chi^{(3)}]$ (-ω-ω-ω) Total	−23.60	−212.06	−0.04	6.94	−4.29	0.64	−38.74	
	% $\lvert\chi^{(3)}\rvert_j$	10	86	0	3	1	0		
ω = 0 s^{-1}	10^{-13} esu								
	$\lvert\chi^{(3)}\rvert$	7.40	69.00	0.01	2.27	1.40	0.22	12.53	192
	% $\lvert\chi^{(3)}\rvert$	10	92	0	3	3	0		
	$\lvert\chi^{(3)}\rvert$ (λ/ω=0)	153	147	267	147	147	143	148	
INTERBAND	$\lvert\chi^{(3)}\rvert$ INTERBAND /								
λ=1064 nm	$\lvert\chi^{(3)}\rvert$TOTAL RiCi	105	95	327	95	97	82	96	
	$\lvert\chi^{(3)}\rvert$a1 INTERBAND/								
	$\lvert\chi^{(3)}\rvert$TOTAL RiCi	113	106	346	53	194	273	110	
LEFT-ROTATORY									
Carbon taken as Reference[e]		5	10	9	8	7	6		
λ = 1064 nm	10^{-13} esu								
	Re $[\chi^{(3)}]$	42.47	−0.12	−0.05	−0.00	−1.53	−1.88	6.48	
	$\lvert\chi^{(3)}\rvert$	42.61	0.12	0.05	0.00	1.56	2.94	6.51	100
	Re $[\chi^{(3)}]$ (-ω-ω-ω)^{1}B	−11.86	0.03	0.01	0.00	0.43	1.24	−1.81	
	Re $[\chi^{(3)}]$ (-ω-ω-ω)La	481.06	−1.33	−0.06	−0.03	−17.32	−21.88	73.31	
	Re $[\chi^{(3)}]$ (-ω-ω-ω) Total	88.81	−0.24	−0.11	0.00	−3.20	−4.02	13.54	
	% $\lvert\chi^{(3)}\rvert_j$	109	0	0	0	4	8		
ω = 0 s^{-1}	10^{-13}esu								
	$\lvert\chi^{(3)}\rvert$	28.44	0.06	0.04	0.00	1.10	1.85	4.39	67
	% $\lvert\chi^{(3)}\rvert$	90	0	0	0	3	6		
	$\lvert\chi^{(3)}\rvert$ (λ/ω=0)	149	192	143	119	143	159	148	
INTERBAND	$\lvert\chi^{(3)}\rvert$ INTERBAND /								
λ=1064 nm	$\lvert\chi^{(3)}\rvert$TOTAL LiCi	99	151	86	39	87	116	97	
	$\lvert\chi^{(3)}\rvert$ a1 INTERBAND /								
	$\lvert\chi^{(3)}\rvert$TOTAL LiCi	12	180	86	39	88	116	25	

[a]The experimental value of o-NA at 1064 nm is 6.53 × 10^{-13} esu. The calculated value at 1064 nm of $\chi^{(3)}$ is −6.0 X 10^{-13} + 2.2 X 10^{-16}. This calculated value is due to the vectorial sum of the right and left circulations, indicating a defocusing behavior.
[b]The total percentage in relationship to the experimental value is 92 % for λ = 1064 nm and 62 % for ω= 0 s^{-1}. The total interband contribution is 96 %.
[c]The transitions are ^{1}B (λ = 230 nm, β_2 = 6.525 eV, η= 0.0034, fosc = 0.7958), and La (λ = 404 nm, β_2 = 3.714 eV, η= 0.0046, fosc = 0.2042).
[d]The Re $[\chi^{(3)}]$ (-ω-ω-ω)^{1}B and Re $[\chi^{(3)}]$ (-ω-ω-ω)^{1}La values correspond to the permutation (-ω-ω-ω) of the ^{1}B and La transitions. See text. The proportions of the oscillator strengths are fosc(^{1}B) = 0.7958, fosc(La) = 0.2042.
[e]For the beginning of the unitary cell.

Table 10
NLO values for m-NA considering the oxygens and nitrogens separated, and also correlation effects.

								Average	% Exp
RIGHT ROTATORY									
Carbon taken as Reference[e]		**5**	**6**	**7**	**8**	**9**	**10**		
$\lambda = 1064$ nmb	10^{-13} esu								
	$Re[\chi^{(3)}]$	0.04	−0.23	−7.27	−2.80	−0.09	−0.15	−1.75	
	$\lvert\chi^{(3)}\rvert$	0.04	0.23	7.27	2.80	0.09	0.15	1.75	97
	$Re[\chi^{(3)}]$ (-ω-ω-ω)^{1}B	−0.02	0.15	4.67	1.79	0.06	0.10	1.12	
	$Re[\chi^{(3)}]$ (-ω-ω-ω)La	1.46	−9.45	−301.79	−116.12	−3.81	−6.23	−72.66	
	$Re[\chi^{(3)}]$ (-ω-ω-ω) Total	0.07	−0.48	−15.43	−5.94	−0.19	−0.32	−3.72	
	% $\lvert\chi^{(3)}\rvert_j$	0	2	69	26	1	1		
$\omega = 0$ s^{-1}	10^{-13} esu								
	$\lvert\chi^{(3)}\rvert$	0.06	0.03	3.06	4.91	0.15	0.49	1.43	79
	% $\lvert\chi^{(3)}\rvert$	1	0	35	56	2	6		
	$\lvert\chi^{(3)}\rvert$ (λ/ω=0)	55	869	237	57	60	31	122	
INTERBAND	$\lvert\chi^{(3)}\rvert$INTERBAND /								
λ=1064 nm	$\lvert\chi^{(3)}\rvert$TOTAL RiCi	21	326	210	23	30	3	159	
	$\lvert\chi^{(3)}\rvert$a1 INTERBAND /								
	$\lvert\chi^{(3)}\rvert$TOTAL RiCi	21	328	216	28	36	0	164	
LEFT-ROTATORY									
Carbon taken as Reference[e]		**5**	**10**	**9**	8	**7**	**6**		
$\lambda = 1064$ nm	10^{-13} esu								
	$Re[\chi^{(3)}]$	0.22	−0.00	−0.00	0.00	−11.67	−0.26	−1.95	
	$\lvert\chi^{(3)}\rvert$	0.22	0.00	0.00	0.00	11.67	0.26	1.95	
	$Re[\chi^{(3)}]$ (-ω-ω-ω)^{1}B	−0.14	0.00	0.00	−0.00	7.48	0.16	1.25	108
	$Re[\chi^{(3)}]$ (-ω-ω-ω)La	9.31	−0.04	−0.00	0.37	−484.69	−10.59	−80.94	
	$Re[\chi^{(3)}]$ (-ω-ω-ω) Total	0.48	−0.00	−0.00	−0.02	−24.78	−0.54	−4.14	
	% $\lvert\chi^{(3)}\rvert_j$	2	0	0	0	100	2		
$\omega = 0$ s^{-1}	10^{-13}esu								
	$\lvert\chi^{(3)}\rvert$	0.31	0.01	0.00	0.00	3.52	0.42	0.61	34
	% $\lvert\chi^{(3)}\rvert$	9	0	0	0	97	11		
	$\lvert\chi^{(3)}\rvert$ (λ/ω=0)	71	7	17	1884	331	61	321	
INTERBAND	$\lvert\chi^{(3)}\rvert$INTERBAND/								
λ=1064 nm	$\lvert\chi^{(3)}\rvert$TOTAL LiCi	49	1032	145	443	904	31	902	
	$\lvert\chi^{(3)}\rvert$ a1 INTERBAND/								
	$\lvert\chi^{(3)}\rvert$TOTAL LiCi	49	1023	145	444	955	31	963	

[a]**The experimental value of m-NA at 1064 nm is 1.81 × 10^{-13} esu. The calculated value at 1064 nm of $\chi^{(3)}$ is −1.9 X 10^{-13} −3.6 X 10^{-16}. This calculated value is due to the vectorial sum of the right and left circulations, indicating a defocusing behavior.**
[b]**The total percentage in relationship to the experimental value is 102 % for $\lambda = 1064$ nm and 56 % for $\omega = 0$ s^{-1}. The total interband contribution is 400 %.**
[c]**The transitions are ^{1}B ($\lambda = 231$ nm, $\beta_2 = 6.413$ eV, η= 0.0001372, fosc = 0.9345), and La ($\lambda = 373$ nm, $\beta_2 = 3.472$ eV, η= 0.000144, fosc = 0.0655).**
[d]**The Re$[\chi^{(3)}]$ (-ω-ω-ω)^{1}B and Re$[\chi^{(3)}]$ (-ω-ω-ω)^{1}La values correspond to the permutation (-ω-ω-ω) of the ^{1}B and La transitions. See text.**
[e]**For the beginning of the unitary cell.**

normalized transition moment by the band gap in Agrawal's methodology $\frac{\partial S_{ij}}{\partial k}$ [1,5] being *i,j = v,c*. *Sij* is given by

$$S_{ij} = \frac{\Omega_{ij}}{\omega_{ij}} \tag{4}$$

Sij indicates that the dependence is on the non-dimensional energy difference between the conduction and the valence band and the transition dipole moment. In this case, the resonance energy β_2 and the non-dimensional difference (ζc-ζv) of the band gap normalize the transition dipole moment.

As observed in Table 8, there is an optical similarity in all the atoms in the nitroanilines o-NA and p-NA, and aniline polyenynes POEo-A and POEp-A because of the similar values of $\Delta\Omega_{i,cv}/(a_{ver}$ e). The only exception is in the nitrogen N11 of the aniline polyenyne POEo-A. This exception can be used in chemical synthesis in order to add a moiety to this nitrogen N11 to change this value and increase the change of the average transition moment for each atom $\Delta\Omega_{i,cv}/(a_{ver}\, e)$. Besides, there is also a similarity in this parameter in the compounds m-NA and POEm-A. For both cases, the dipole moment change for each atom indicates a similarity in optical behavior associated with resonances and wavefunctions.

3.4. $\chi^{(3)}$ values

We have evaluated the value of $\chi^{(3)}$ in this model with the values of the $\chi^{(3)}$ of the different experimental bands weighted by the proportion of their oscillator strengths, for example, for m-NA [4]:

$$\chi^{(3)}_{Total,m-NA} = \left(f_{i,^1B}\chi^{(3)}_{^1B} + f_{i,La}\chi^{(3)}_{La}\right) \tag{5}$$

Also, we have considered the Right and Left rotatory circulations of the electrons in the aromatic ring with transition moments from the carbons in this aromatic ring (6 on the left: carbon C5 to carbon C10, and six on the right: carbon C5 to carbon C6 as seen in Tables 9, 10, 11), the effect of phonons, and interband and intraband effects [4]. In this work, we have also considered the separated influence of the nitro group's oxygens and nitrogen and the correlation effects on the $\chi^{(3)}$ values. When we observe Tables 9, 10, and 11, we realize that the phononic factor η is near 0.003 for o-NA, almost zero for m-NA, and 0.02 for p-NA. The low value of the phononic factor in o-NA and m-NA produces the imaginary value of $\chi^{(3)}$ to be 3 orders of magnitude lower than the real-$\chi^{(3)}$ value, as seen in these tables. This low value of the imaginary part of $\chi^{(3)}$ indicates that the energy loss by the $\chi^{(3)}$ nonlinear properties is negligible. Conversely, the imaginary value of $\chi^{(3)}$ in p-NA is only one order of magnitude less than the real-$\chi^{(3)}$ value, as expected by a higher phononic component, as seen in Table 9. Besides, we consider that the high number of stable resonance structures in o-NA and p-NA produces a similar weight of the Left and Right rotatory circulation [4]. For this reason, the relation $\lvert\chi^{(3)}\rvert$ **(λ/ω=0)** of the Left and Right circulation is the same in both directions: 148% and 914 %, respectively, as seen in Tables 9 and 11. This similarity of the Left and Richt circulation is not the case for m-NA, in which the Right rotatory circulation has a $\lvert\chi^{(3)}\rvert$ **(λ/ω=0)** ratio of 122 % and the Left rotatory circulation a ratio of 321%.

Table 11
NLO values for p-NA considering the oxygens and nitrogens separated, and also correlation effects.

								Average	% Exp
RIGHT ROTATORY									
Carbon taken as Reference[e]		**5**	**6**	**7**	**8**	**9**	**10**		
λ = 1064 nmb	**10^{-13} esu**								
	Re[$\chi^{(3)}$]	**−4.44**	**−3.64**	**−0.22**	**−40.50**	**6.52**	**−14.73**	**−9.50**	
	$\lvert\chi^{(3)}\rvert$	**4.49**	**3.94**	**0.25**	**41.26**	**17.75**	**15.10**	**9.52**	**111**
	Re[$\chi^{(3)}$] (-ω-ω-ω)^{1}B$_{11}$	**0.07**	**0.06**	**0.00**	**0.68**	**−0.17**	**0.25**	**0.15**	
	Re[$\chi^{(3)}$] (-ω-ω-ω)^{1}B$_{12}$	**0.15**	**0.13**	**0.00**	**1.38**	**−0.34**	**0.50**	**0.30**	
	Re[$\chi^{(3)}$] (-ω-ω-ω)La	**−9.85**	**−8.15**	**−0.48**	**−89.97**	**15.70**	**–32.75**	**−20.92**	
	Re[$\chi^{(3)}$] (-ω-ω-ω) Total	**−5.22**	**−4.32**	**−0.25**	**−47.67**	**8.28**	**−17.35**	**−11.09**	
	$\lvert\chi^{(3)}\rvert_j$	**5**	**5**	**0**	**50**	**21**	**18**		
ω = 0 s^{-1}	**10^{-13} esu**								
	$\lvert\chi^{(3)}\rvert$	**0.49**	**0.48**	**0.03**	**4.52**	**1.94**	**1.65**	**1.04**	**12**
	% $\lvert\chi^{(3)}\rvert$	**5**	**5**	**0**	**50**	**21**	**18**		
	$\lvert\chi^{(3)}\rvert$ (λ/ω=0)	**914**	**914**	**914**	**914**	**914**	**914**	**914**	
INTERBAND	**$\lvert\chi^{(3)}\rvert$ INTERBAND /**								
λ=1064 nm	**$\lvert\chi^{(3)}\rvert$TOTAL RiCi**	**15**	**25**	**1**	**7**	**137**	**19**	**38**	
INTRABAND	**$\lvert\chi^{(3)}\rvert$b1 INTRABAND/**								
λ=1064 nm	**$\lvert\chi^{(3)}\rvert$TOTAL RiCi**	**113**	**63**	**76**	**89**	**76**	**75**	**120**	
LEFT-ROTATORY									
Carbon taken as Reference[e]		**5**	**10**	**9**	**8**	**7**	**6**		
λ = 1064 nm	**10^{-13} esu**								
	Re[$\chi^{(3)}$]	**4.41**	**−5.36**	**0.48**	**7.99**	**22.49**	**−16.72**	**−5.0.28**	
	$\lvert\chi^{(3)}\rvert$	**6.33**	**5.83**	**0.49**	**8.65**	**22.94**	**16.74**	**5.38**	**63**
	Re[$\chi^{(3)}$] (-ω-ω-ω)^{1}B$_{11}$	**−0.08**	**0.09**	**−0.00**	**−0.11**	**0.38**	**0.27**	**0.09**	
	Re[$\chi^{(3)}$] (-ω-ω-ω)^{1}B$_{12}$	**−0.18**	**0.19**	**−0.02**	**−0.23**	**0.77**	**0.55**	**0.18**	
	Re[$\chi^{(3)}$] (-ω-ω-ω)La	**10.09**	**−12.01**	**1.06**	**17.37**	**−49.97**	**−39.94**	**−11.73**	
	Re[$\chi^{(3)}$] (-ω-ω-ω) Total	**5.34**	**−6.36**	**0.56**	**9.21**	**−26.48**	**−19.58**	**−6.22**	
	% $\lvert\chi^{(3)}\rvert_j$	**20**	**18**	**2**	**27**	**71**	**52**		
ω = 0 s^{-1}	**10^{-13}esu**								
	$\lvert\chi^{(3)}\rvert$	**0.69**	**0.64**	**0.00**	**0.95**	**2.61**	**1.81**	**0.59**	**7**
	% $\lvert\chi^{(3)}\rvert$	**10**	**10**	**1**	**14**	**38**	**27**		
	$\lvert\chi^{(3)}\rvert$ (λ/ω=0)	**914**	**914**	**914**	**914**	**914**		**914**	
INTERBAND	**$\lvert\chi^{(3)}\rvert$ INTERBAND /**								
λ=1064 nm	**$\lvert\chi^{(3)}\rvert$TOTAL LiCi**	**130**	**102**	**105**	**158**	**7**	**62**	**7**	
INTRABAND	**$\lvert\chi^{(3)}\rvert$ b1 INTRABAND/**								
λ=1064 nm	**$\lvert\chi^{(3)}\rvert$TOTAL LiCi**	**58**	**21**	**10**	**65**	**83**	**54**	**119**	

[a]The experimental value of p-NA at 1064 nm is 8.55 × 10^{-13} esu. The calculated value at 1064 nm of $\chi^{(3)}$ is −7.9 X 10^{-13} −2.5 X 10^{-5}. This calculated value is due to the vectorial sum of the right and left circulations, indicating a defocusing behavior.
[b]The total percentage in relationship to the experimental value is 86 % for λ = 1064 nm and 9 % for ω= 0 s^{-1}. The total interband contribution is 27 %.
[c]The transitions are ^{1}B$_{11}$ (λ = 203 nm, β_2 = 7.018 eV, η= 0.01692, fosc = 0.1711), ^{1}B$_{12}$ (λ = 231 nm, β_2 = 6.167 eV, η= 0.016968, fosc = 0.2933), and La (λ = 372 nm, β_2 = 3.829 eV, η= 0.016846, fosc = 0.5356).
[d]The Re[$\chi^{(3)}$] (-ω-ω-ω)^{1}B$_{11}$, Re[$\chi^{(3)}$] (-ω-ω-ω)^{1}B$_{12}$, and Re[$\chi^{(3)}$] (-ω-ω-ω)^{1}La values correspond to the permutation (-ω-ω-ω) of the ^{1}B$_{11}$, ^{1}B$_{12}$, and La transitions. See text.
[e]For the beginning of the unitary cell.

On the other hand, the interband and intraband effects with a low variation of the dipole moment in o-NA, middle in m-NA, and high in p-NA associated with correlation effects, as seen above, produce that the interband contribution is 96 % in o-NA, 400 % in m-NA, and 27 % in p-NA. The high percentage of the interband contribution in m-NA indicates the opposite sign of the intraband contribution. As observed in **Eqs. (14) and (15)**, and Tables 9, 10, and 11, the interband term a1 is the most critical contribution to o-NA in the Right rotatory circulation (110 % to total interband 96%) and the less significant term in the Left rotatory circulation (25% to the total interband 97%). In m-NA, the term a1 is the most important in the interband contribution (164 % in the Right rotatory circulation and 963 % in the Left rotatory circulation). In p-NA, the term b1, which takes into account the derivative of the dipole moment, the second derivative of the wavefunction coefficients as seen in **Reference** [5], has the most influence (120 % and 119 %, respectively).

About the most predominant contributions in the Right and Left rotatory circulations to the value of $\chi^{(3)}$ of the moments from the carbons in the aromatic ring[j]: a). from carbon C6 in Right rotatory circulation R2C6 (86 %) and carbon C5 in the Left rotatory circulation L1C5 (109 %) in o-NA as seen in Table 9; Similarly, b). R3C7 (69%), R4C8(26%), L5C7 (100%) in m-NA as seen in Table 10; c). R4C8 (50%), R5C9(21%), R6C10 (18%), L4C8 (27%), L5C7(71%), L6C6 (52%) in p-NA as seen in Table 11. Then, the higher the intraband contribution associated with the variation of the dipole moments due to correlation effects, the higher the number of carbons that contributes to the value of $\chi^{(3)}$ in the sequence o-NA, m-NA, and p-NA.

About the defocusing behavior with Re($\chi^{(3)}$) < 0 [13], the real part of the $\chi^{(3)}$ value is negative in all the nitroanilines o-NA, m-NA, and p-NA as observed in Tables 9, 10, and 11. Through **Eq. (5)** and the above discussion, the defocusing behavior depends mainly on the proportion of the oscillator strengths of the experimental bands, the right and left circulation of the electrons in the aromatic ring, and the transition moments from the carbons in the aromatic ring. Table 9 shows the dependence of the negative value of the real part of $\chi^{(3)}$ on these factors in o-NA. On the other hand, from all the permutations in the evaluation of $\chi^{(3)}$ at λ_{Laser} = 1064 nm, as explained below, the most crucial contribution to $\chi^{(3)}$ comes from the permutation 008 $-\omega-\omega-\omega$, as seen in Tables 9, 10, and 11. This permutation is at 3ω of λ_{Laser} = 1064 nm, that is, 357 nm, and this value is near the frequency of the transition La (373 nm) of p-NA, as explained in Table 11. Then, there is a high resonance at this wavelength, and in consequence, there is a dispersion of the light and a high variation of $\chi^{(1)}$, as seen, for example, in **Reference** [4]. Also, through the approximation that $\chi^{(1)}$^4 is proportional to $\chi^{(3)}$ [14] given by Boyd, we can conclude that the real values of $\chi^{(3)}$ are negative if they are close to these resonances. In this way, **Fig. S11** of Supplementary Information plots the values $\chi^{(1)}$ for p-NA, taking into account that the value of $\chi^{(3)}$ in the permutation $-\omega-\omega-\omega$ with λ_{Laser} =

1064 nm (resonance at $3\omega = 354$ nm) is negative for the carbon C5 in Right rotatory circulation R1C5. The real value of $\chi^{(3)}$ from this carbon C5 in the transition La is Re[$\chi^{(3)}$] (-ω-ω-ω)La = -9.85 X 10^{-13} esu, as seen in Table 11. Correspondingly, the value of $\chi^{(1)}$ at 354 nm is $-0.0058 - i\,0.0012$. Considering that $\chi^{(1)} = a - bi$, then negative values of $\chi^{(3)}$ are obtained if $2a^2b^2 > a^4 + b^4$ by the approximation of Boyd. Indeed, from the values of $\chi^{(1)}$ in **Fig. S11**, we have negative values of $\chi^{(3)}$ in all the range of values of this figure. These negative values are the case for the contribution from the transition of one carbon, in this case, C5, in the Right rotatory circulation. On the other hand, the total contribution of the Left and Right rotatory contributions on the defocusing can be opposite, for example, in o-NA: Re[$\chi^{(3)}$] (-ω-ω-ω)Total = -38.74 X 10^{-13} in Right rotatory circulation, and Re[$\chi^{(3)}$] (-ω-ω-ω)Total = 13.54 X 10^{-13} in Left rotatory circulation. In m-NA and p-NA, the Right and Left rotatory circulatory contributions are negative, as seen in Tables 10 and 11. Tables 9, 10, and 11 note the importance of the weight of the proportion of the oscillator strengths of the bands in the total value of Re [$\chi^{(3)}$] (-ω-ω-ω)Total.

3.4.1. *Light absorption and Laser intensity aspects in the increase of $\chi^{(3)}$.*

In the analysis of the physical factors that affect the evaluated value of $\chi^{(3)}$, we consider the equation of de Amore [15] for the Marker Fringe's method of the THG technique for a film:

$$\chi^{(3)}_{Film} \propto \chi^{(3)}_{S} \left(\frac{2I^{S}_{c}}{\pi} \frac{\alpha_{3\omega}/2}{(1-\exp(-\alpha_{3\omega} l_{Film}/2))} \right) \left(\frac{I^{Film}_{3\omega}}{I^{S}_{3\omega}} \right)^{1/2} \quad (6)$$

As observed, the value of $\chi^{(3)}$ depends on the value of the absorption coefficient α which can change by absorption saturation, phase-space filling, and conformational deformation in conjugated polymers, as explained by Prasad and Williams [16]. The phase matching influences the intensity due to the equalization of the refraction index between the incident laser light and the NLO light generated [14,17]. This intensity can be increased by the rotation angle, as happens in the birefringent crystal guanidinium tetrafluoroborate for SHG [18], or by the temperature [16]. Indeed, if the intensity of the standard S increases by the phase matching in the same proportion, the evaluated value of $\chi^{(3)}$ does not increase, as observed through **Eq. (5)**, but if the film increases its intensity more than the standard S, then the evaluated value of $\chi^{(3)}$ increases.

4. Conclusions

In the search for factors that influence the $\chi^{(3)}$ values, the different physicochemical levels and instrumental techniques can improve the finding of model compounds with better $\chi^{(3)}$-characteristics. We have found that the coordination of the elements of an ensemble or the weight of its most significant elements, such as the sequence of the same sign of charge on the closest atoms or the nitrogen of the amine, respectively, gives insights into how to increase the NLO properties. In this way, the configurational distribution of charges and charge density, the dipole moments with their interband effects, the physicochemical constitutive global factors to determine the $\chi^{(3)}$ values, and the interaction of the laser light with the sample help increase the $\chi^{(3)}$ values. This search of physicochemical factors also lets us know the importance of the carbon joined to the enyne or the nitro groups as a reservoir source that allows the change of charge of these groups. We have also corroborated that the NLO properties can be extrapolated from the linear optical properties, as is the case of the defocusing behavior. Significantly, this analysis can be extended to other aromatic substituents, for example hydroxy phenyl derivatives in porphyrines [19] or pyrene with aldehyde as D-π-A system [20]; three functional groups: phenyl, nitro, and hydroxy [21]; in crystals with elements such as B, N, Li, O in a DFT study [22] or of Se, Ge, Zn and Cu [23], even in NLO ferromagnetic materials [24]. Besides, this methodology promotes correlating specific NLO properties as mid-infrared NLO properties [25] or a strong exciton in quantum wells [26] to the distribution of charges, charge density, or the influence of intraband dipole moments.

Declaration of Competing Interest

The authors declare that they have no known competing financial interests or personal relationships that could have appeared to influence the work reported in this paper.

Data availability

The computational programs required to reproduce these findings cannot be shared at this time as the computer programs also forms part of an ongoing study.

Acknowledgments

We thank the commentaries on the work of Dr. Humberto Vázquez Torres and the suggestions of Dr. Raúl Arzate Romero from the UAM Iztapalapa. We are very grateful for using the supercomputer cluster Yoltla-LANCAD, which Laboratorio de Súpercomputo y Visualización en Paralelo (LSVP) at UAM-I maintains (grant 25-2023). Dr. Cesar A. Guarin and Dr. Luis Mendoza-Luna acknowledge CONAHCYT for grant-683-Investigadores por México (formerly Cátedra-CONACYT). We acknowledge Reviewer 2's suggestion regarding the influence of birefringent standards on evaluating $\chi^{(3)}$.

Appendix A. Equations

A.1. *Wavefunctions and Dipole Moment*

The following wavefunction equation for the Right rotatory circulation R1C5 [**4**] helps to evaluate the dipole moment for p-NA:

$$\Psi_j(n,k) = \frac{1}{(10N)^{1/2}} \sum_{j=1}^{10} \sum_{n=1}^{N} exp(i3nka) \left(c_{2j}\phi_{-2}e^{-i3\theta/2} + c_{3j}\phi_{-2}e^{-i3\theta/2} + c_{4j}\phi_{-1}e^{-i0.6\theta} + c_{5j}\phi_0 + c_{6j}\phi_1 e^{i0.56\theta} + c_{7j}\phi_2 e^{i1.12\theta} + c_{8j}\phi_3 e^{i1.68\theta} + N_{11j}\phi_4 e^{i2.24\theta} + c_{9j}\phi_4 e^{i2.80\theta} + c_{10j}\phi_5 e^{i3.36\theta} \right) \quad (7)$$

being j the band energy, n the number of cells, and k the wavenumber. These expressions come from Sutton's methodology, and Agrawal's methodology deletes the phase factors [**5**]:

For evaluating the dipole moment, we use:

$$\Omega_{ij} = \lim_{n\to 1\ N\to 1} [\int u_{ik}^{*}(\frac{\partial u_{jk}}{\partial k})dx] \tag{8}$$

With:

$$u_{kj}(x) = \exp(ikx)\psi_j(k) \tag{9}$$

And using:

$$\int \phi_n ex \phi_{n'} d\tau = e\frac{na}{2}\delta_{n.n'} \tag{10}$$

The resultant expression considering valence band $v = 6$ and conduction band $c = 1$ is considering the wavefunction coefficients from the carbon C5 in the Right rotatory circulation in p-NA R1C5:

$$\Omega_{16} = \left(\frac{i}{2}\left(8c_{21}^{*}c_{46} + 8c_{31}^{*}c_{36} + 7c_{41}^{*}c_{46} + 6c_{51}^{*}c_{56} + 5c_{61}^{*}c_{66} + 4c_{71}^{*}c_{76} + 3c_{81}^{*}c_{86} + 2c_{91}^{*}c_{96} + 1c_{101}^{*}c_{106} + 3c_{111}c_{116}\right) + (c_{21}^{*}\frac{\partial c_{26}}{d\theta} + c_{31}^{*}\frac{\partial c_{36}}{d\theta} + c_{41}^{*}\frac{\partial c_{46}}{d\theta} + c_{51}^{*}\frac{\partial c_{56}}{d\theta} + c_{61}^{*}\frac{\partial c_{66}}{d\theta} + c_{71}^{*}\frac{\partial c_{76}}{d\theta} + c_{81}^{*}\frac{\partial c_{86}}{d\theta} + c_{91}^{*}\frac{\partial c_{96}}{d\theta} + c_{101}^{*}\frac{\partial c_{106}}{d\theta} + c_{111}^{*}\frac{\partial c_{116}}{d\theta})\right)\frac{a}{2} \tag{11}$$

For the aromatic polyenyne POEp-A, the wavefunction is:

$$\Psi_j(n,k) = \frac{1}{(11N)^{1/2}}\sum_{j=1}^{11}\sum_{n=1}^{N} exp(i2nka)\left(c_{1j}\phi_{4n-3} + c_{2j}\phi_{4n-2}e^{i\theta/2} + c_{3j}\phi_{4n-1}e^{i\theta} + N_{4j}\phi_{4n}e^{i3\theta/2} + c_{5j}\phi_{4n}e^{i1.1\theta} + c_{6j}\phi_{4n}e^{i1.66\theta} + c_{7j}\phi_{4n}e^{i2.22\theta} + c_{8j}\phi_{4n}e^{i2.78\theta} + N_{11j}\phi_{4n}e^{i3.28\theta} + c_{9j}\phi_{4n}e^{i2.22\theta} + c_{10j}\phi_{4n}e^{i1.66\theta}\right) \tag{12}$$

The resultant dipole transition between the valence band $v = 6$ and the conduction band $c = 1$ is:

$$\Omega_{16} = \left(\frac{i}{2}\left(3c_{11}^{*}c_{16} + 2c_{21}^{*}c_{26} + 1c_{31}^{*}c_{36}\right) + \left(c_{11}^{*}\frac{\partial c_{16}}{d\theta} + c_{21}^{*}\frac{\partial c_{26}}{d\theta} + c_{31}^{*}\frac{\partial c_{36}}{d\theta} + c_{41}^{*}\frac{\partial N_{46}}{d\theta} + c_{51}^{*}\frac{\partial c_{56}}{d\theta} + c_{61}^{*}\frac{\partial c_{66}}{d\theta} + c_{71}^{*}\frac{\partial c_{76}}{d\theta} + c_{91}^{*}\frac{\partial c_{96}}{d\theta} + c_{101}^{*}\frac{\partial c_{106}}{d\theta} + c_{111}^{*}\frac{\partial N_{116}}{d\theta})\right)\frac{a}{2} \tag{13}$$

This expression is similar to the aromatic polyenyne with an aniline moiety in ortho position POEo-A; only the values of the coefficients are different. We must also remark that the dipole moment from a particular atom in nitroanilines has the contribution of all the atoms, as observed in **Eq. (11)**. As seen, in the aromatic polyenynes, the dipole moment does not depend on a reference atom but on all atoms, as explained above. Also, as observed, the dipole moments depend on two parts: an integral value of the wavefunction coefficient, which we associate with the interband part. The other part of the equations is the derivate of the wavefunction coefficient of the departure band with the conjugate of the wavefunction coefficient of the final state of the transition, which we associate with the intraband contribution. Indeed, if we evaluate the intraband transition Ωvv and Ωcc, the dipole moments in the interband contribution are associated with the square of the wavefunction coefficients and the charge density Ci^2. In this way, the product of the wavefunction coefficient of the valence band and the complex conjugate of the wavefunction coefficient of the conduction band gives the transition dipole moment Ωcv in the interband contribution.

A.2. $\chi^{(3)}$

Equations:

$$\chi^{(3)}_{xxxx,interband} = \chi_0^{(3)}\int_{-\pi/a}^{\pi/a} dk\left\{\frac{(\Omega_{vv}f_v^{0.5}g_v^{0.5} - \Omega_{cc}f_c^{0.5}g_c^{0.5})^2}{\omega_{vc}}S_{vc}S_{cv}g_c^{0.5}g_v^{0.5}f_{vc}^{0.5}f_{cv}^{0.5} + \Omega_{vc}S_{cv}S_{vc}S_{cv}g_cg_vf_{vc}f_{cv}\right\} = a_{1,c(3)} + a_{2,c(3)} \tag{14}$$

$$\chi^{(3)}_{xxxx,intraband} = \chi_0^{(3)}\int_{-\pi/a}^{\pi/a} dk[\ \frac{1}{\omega_{cv}}\frac{\partial S_{vc}}{\partial k}\frac{\partial S_{cv}}{\partial k}f_{vc}f_{cv}g_cg_v + \frac{(\Omega_{vv}f_{vv}^{0.5}g_{vv}^{0.5} - \Omega_{cc}f_{cc}^{0.5}g_{cc}^{0.5})}{\omega_{cv}}\left[S_{vc}\frac{\partial S_{cv}}{\partial k}f_{vc}^{0.5}f_{cv}g_v^{0.5}g_c - S_{cv}\frac{\partial S_{vc}}{\partial k}f_{cv}^{0.5}f_{vc}g_c^{0.5}g_v\right]\ ] = b_{1,c(3)} + b_{2,c(3)} \tag{15}$$

$$\chi^{(3)}_{xxxx} = \chi^{(3)}_{xxxx,interband} + \chi^{(3)}_{xxxx,intraband} \tag{16}$$

Where:

$$\chi_0^{(3)} = \frac{32\pi^2e^4\sigma}{h^3a} \tag{17a}$$

Posteriorly, by substitution of the other variables, is changed:

$$\chi_0^{(3)} = \frac{8e^4\sigma a^3}{\beta_2^3\pi} \tag{17b}$$

For $\omega \neq 0$, following Agrawal and Flytzanis, and again considering the energy degeneracy.

$$\chi^{(3)}_{xxxx,interband} = \frac{e^4\sigma}{\hbar^3 2\pi a}\int_{-\pi/a}^{\pi/a} dk\sum_{\boldsymbol{P}}\left\{\frac{\Omega_{vc}[(\Omega_{vv}f_{vv}^{0.5}g_v^{0.5} - \Omega_{cc}f_{cc}^{0.5}g_c^{0.5})^2f_{vc}^{0.5}f_{cv}^{0.5}g_v^{0.5}g_c^{0.5} - \Omega_{cv}\Omega_{vc}g_cg_vf_{vc}f_{cv}]\Omega_{cv}}{(\omega_{cv} + \omega_1 + \omega_2 + \omega_3 + i\frac{\Gamma}{2})(\omega_{cv} + \omega_2 + \omega_3 + i\frac{\Gamma}{2})(\omega_{cv} + \omega_3 + i\frac{\Gamma}{2})}\right\} \tag{18}$$

$$\chi^{(3)}_{xxxx,intraband} = \frac{e^4\sigma}{\hbar^3 2\pi a}\int_{-\pi/a}^{\pi/a} dk \sum_{\boldsymbol{P}} \left\{ \frac{-1}{\left(\omega_{cv}+\omega_1+\omega_2+\omega_3+i\frac{\Gamma}{2}\right)} \frac{\partial}{\partial k}\left(\frac{\Omega_{vc}}{\left(\omega_{cv}+\omega_2+\omega_3+i\frac{\Gamma}{2}\right)}\right) \frac{\partial}{\partial k}\left(\frac{\Omega_{cv}}{\left(\omega_{cv}+\omega_3+i\frac{\Gamma}{2}\right)}\right) f_{vc}f_{cv}g_v g_c \right.$$
$$+ \frac{\left(\Omega_{vv}f_{vv}^{0.5}g_v^{0.5} - \Omega_{cc}f_{cc}^{0.5}g_c^{0.5}\right)}{\left(\omega_{cv}+\omega_1+\omega_2+\omega_3+i\frac{\Gamma}{2}\right)}\left[\frac{\Omega_{cv}}{\left(\omega_{cv}+\omega_3+i\frac{\Gamma}{2}\right)} \frac{\partial}{\partial k}\left(\frac{\Omega_{vc}}{\left(\omega_{cv}+\omega_2+\omega_3+i\frac{\Gamma}{2}\right)}\right) f_{cv}^{0.5}f_{vc}g_c^{0.5}g_v \right.$$
$$\left.\left. - \frac{\Omega_{vc}}{\left(\omega_{cv}+\omega_2+\omega_3+i\frac{\Gamma}{2}\right)} \frac{\partial}{\partial k}\left(\frac{\Omega_{cv}}{\left(\omega_{cv}+\omega_3+i\frac{\Gamma}{2}\right)}\right) f_{vc}^{0.5}f_{cv}g_v^{0.5}g_c \right] \right\} \tag{19}$$

f_{cv} is the number of transition moments from the valence band to the conduction band, and g_c is the degeneracy of the conduction band level, the same applied to the conduction band transition to the valence band. The key to the exponentiation of these factors is that the square of the dipole moment Ω_{ij} is proportional to f_{ij} and g_i as given by the Fermi Gold Rule, as explained in **Reference [4]** . In this work, because there is no degeneracy of the number of transition moments and the number of the bands in the aromatic polyenynes, the coefficients f_{ij} and g_i are equal to 1. Then, **Eqs. (14), (15), (18), (19), (20),** and **(21)** simplifies to the Agrawal's expressions [**1**]. In the case of nitroanilines, we consider that these variables f_{ij} and g_i can take values different from 1. Also, "*P*" indicates the total permutations, which are 8 for a *1*-dimensional chain, and result from the permutations of ω_1, ω_2, and ω_3 between the values $+\omega$ or $-\omega$ (2 X 2 X 2). Besides, because we have considered that the aromatic polyenynes are linear chains, the fourth-rank tensor $\chi^{(3)}_{xxxx}$ becomes a zero-rank tensor, $\chi^{(3)}_{xxxx} = \chi^{(3)}$, a complex number.

A.3. Linear Optics

In the case of $\chi^{(1)}$ for asymmetric substances:

$$\chi^{(1)}_{xx,interband} = \chi^{(1)}_0 \int_{-\pi/a}^{\pi/a} dk \left(\frac{-\omega_{cv}\Omega_{vc}(k)\Omega_{cv}(k) f_{cv}^{0.5}f_{vc}^{0.5}g_c^{0.5}g_v^{0.5}}{\omega_{cv}^2 - \left(\omega - i\frac{\Gamma}{2}\right)^2} \right) \tag{20}$$

In the case of symmetric substances with $\Omega_{cv} = -\Omega_{vc}^*$:

$$\chi^{(1)}_{xx,interband} = \chi^{(1)}_0 \int_{-\pi/a}^{\pi/a} dk \left(\frac{\omega_{cv}|\Omega_{cv}(k)|^2 g_c f_{cv}}{\omega_{cv}^2 - \left(\omega - i\frac{\Gamma}{2}\right)^2} \right) \tag{21}$$

$$\chi^{(1)}_0 = \frac{4e^2\sigma}{h} \tag{22a}$$

Which then changes to:

$$\chi^{(1)}_0 = \frac{2e^2\sigma a}{8\beta_2} \tag{22b}$$

Appendix B. Supplementary material

Supplementary data to this article can be found online at https://doi.org/10.1016/j.mseb.2023.117016.

References

[1] a) G.P. Agrawal, C. Cojan, C. Flytzanis, Phys. Rev. B 17 (1978) 776–789, https://doi.org/10.1103/PhysRevB.17.776;
b) C. Cojan, G.P. Agrawal, C. Flytzanis, Phys. Rev. B 15 (1977) 909–925, https://doi.org/10.1103/PhysRevB.15.909;
c) C.P. Agrawal, C. Flytzanis, Chem. Phys. Lett. 44 (1976) 366–370, https://doi.org/10.1016/0009-2614(76)80532-5.

[2] H.S. Nalwa, in: H.S. Nalwa, S. Miyata (Eds.) Nonlinear optics of organic molecules and polymers, CRC Press, Florida, 1997, pp. 560-562.

[3] J.A. Díaz-Ponce, Opt. Mat. 66 (2017) 595–604, https://doi.org/10.1016/j.optmat.2017.02.017.

[4] C.A. Guarin, J.A. Díaz Ponce, ACS Omega 5 (2020) 518–528, https://doi.org/10.1021/acsomega.9b03063.

[5] C.A. Guarin, L.G. Mendoza-Luna, J.L. Hernández-Pozos, J.A. Diaz-Ponce, To be published.

[6] a) J.A. Pople, D.L. Beveridge, Approximate Molecular Orbital Theory, Mc Graw Hill Inc., New York, 1970;
b) J.A. Pople, Trans. Farad. Soc. 49 (1957) 1375–1385, https://doi.org/10.1039/TF9534901375;
c) J.A. Pople, D.P. Santry, G.A. Segal, J. Chem. Phys. 43 (1965) S129–S135, https://doi.org/10.1063/1.1701475;
d) J.A. Pople, G.A. Segal, J. Chem. Phys. (1966) 3289–3296, https://doi.org/10.1063/1.1727227.

[7] H.J. Kopineck, Zeitsch. Naturforsch. 5 (1950) 420–431, https://doi.org/10.1515/zna-1950-0802.

[8] Cambridge Crystallographic Center, Accessed 3/08/2019: (a) o-NA: Nieger 2008, https://doi.org/10.5517/ccpzxwf; (b) m-NA: M.R. Probert, C.M. Robertson, J. A. Coome, J. A. K. Howard, B.C. Michell, A.E. Goeta, 2015, https://doi.org/10.5517/cc1jxz6m; (c) p-NA: M. Nieger 2008, https://doi.org/10.5517/ccq45vv.

[9] R. Pariser, R.G. Parr, J. Chem. Phys. 21 (1953) 466–471, https://doi.org/10.1063/1.1698929.

[10] a) V.I. Minkin, O.A. Osipov, Y.A. Zhdanov, Dipole Moments in Organic Chemistry, Plenum Press, London, 1970;
b) O. Exner, Dipole Moments in Organic Chemistry, George Thieme Publishers, Stuttgart, 1975;
c) G. del Re, J. Chem. Soc. (1958) 4031–4040, https://doi.org/10.1039/JR9580004031;
d) G. del Re, B. Pullman, T. Yanezawa, Biochim. Biophys. Acta 75 (1963) 153–182, https://doi.org/10.1016/0006-3002(63)90595-X.

[11] a) G.R. Meredith, J.G. VanDusen, D.J. Williams, Macromolecules 15 (1982) 1385–1389, https://doi.org/10.1021/ma00233a033;
b) K.D. Singer, J.E. Sohn, S.J. Lalama, Appl. Phys. Lett. 49 (1986) 248–250, https://doi.org/10.1063/1.97184;
c) F. Michelotti, E. Toussaere, Opt. Mat. 1–4 (1998) 299–306, https://doi.org/10.1016/S0925-3467(97)00077-3.

[12] C.A. Guarin, L.G. Mendoza-Luna, J.F. Galicia-López, E. Haro-Poniatowski, J. A. Diaz-Ponce, J.L. Hernández-Pozos, Chem. Sel. 8 (2023) e202300524, https://doi.org/10.1002/slct.202300524.

[13] Y.Z. Yu, K.Y. Wong, A.F. Garito, Introduction to nonlinear optics, in: H.S. Nalwa, S. Miyata (Eds.), Nonlinear Optics of Organic Molecules and Polymers, CRC Press, Florida, 1997.
[14] R.W. Boyd, Nonlinear Optics, Academic Press, New York, 1991.
[15] F. D'Amore, A. Zappettini, G. Facchini, S.M. Pietralunga, M. Martinelli, C. Dell'Erba, C. Cuniberti, D. Comoretto, G. Dellepiane, Synth. Met. 127 (2002) 143–146, https://doi.org/10.1016/S0379-6779(01)00605-1.
[16] P.N. Prasad, D.J. Williams, Introduction to nonlinear optical effects in molecules and polymers", John Wiley & Sons, New York, 1991, p. 489.
[17] M. Fox, Optical properties of solids, 1st Edition,, Oxford University Press, New York, 2001, pp. 241–243.
[18] a) M. Mutailipu, J. Han, Z. Li, F. Li, J. Li, F. Zhang, X. Long, Z. Yang, S. Pan 17 (2023) 694–701, https://doi.org/10.1038/s41566-023-01228-7;
b) C. Jin, H. Zeng, F. Zhang, H. Qiu, Z. Yang, M. Mutailipu, S. Pan, Chem. Mater. 34 (2022) 440–450, https://doi.org/10.1021/acs.chemmater.1c03974.
[19] R. Beniwal, P. Gawas, C.P. Charan, V. Nutalapat, B.M.K. Mariserla, Mater. Sci. Eng., B 284 (2022), 115908, https://doi.org/10.1016/j.mseb.2022.115908.
[20] X. Wang, D. Wang, H. Gao, Z. Yang, H. Cao, H. Yang, W. He, H. Wang, J. Gu, H. Hu, J. Nonlinear Opt. Phys. Mater. 25 (2016) 1650014, https://doi.org/10.1142/S0218863516500144.
[21] R. Gandhimathi, R. Dhanasekaran, IOP Conf. Ser.: Mater. Sci. Eng. 43 (2013), 012004, https://doi.org/10.1088/1757-899X/43/1/012004.
[22] A.R. Ayub, R.A. Shehzad, S.S. Alarfaji, J. Iqbal, J. Nonlinear Opt. Phys. Mater. 29 (2020) 2050004, https://doi.org/10.1142/S0218863520500046.
[23] C.W. Sinagra III, F.O. Saouma, C.O. Otieno, S.H. Lapidus, J.-H. Zhang, A.J. Craig, P. Grima-Gallardo, J.A. Brant, K.A. Rosmus, K.E. Rosello, J.I. Jang, J.A. Aitken, J. Alloys Compd. 888 (2021), 161499, https://doi.org/10.1016/j.jallcom.2021.161499.
[24] G. de Luca, M. Fiebig, Phys. Rev. Research 5 (2023), 043055, https://doi.org/10.1103/PhysRevResearch.5.043055.
[25] V. Nguyen, B. Ji, K. Wu, B. Zhang, J. Wang, Chem. Sci. 13 (2022) 2640, https://doi.org/10.1039/D1SC06849K.
[26] E. Hanamura, N. Nagaosa, M. Kumagai, T. Takagahara, Mater. Sci. Eng., B 1 (2022) 255–258, https://doi.org/10.1016/0921-5107(88)90006-2.